Journal of GeoEngineering, Vol. 13, No. 4, pp. 161-170, December 2018
http://dx.doi.org/10.6310/jog.201812_13(4).1

EFFECTS OF PARTICLE SIZE DISTRIBUTIONS AND PRINCIPAL STRESS AXIS ROTATION ON CYCLIC PLASTIC DEFORMATION CHARACTERISTICS OF COARSE MATERIALS

Biyanvilage Dareeju [1], Chaminda Gallage [2*], Tatsuya Ishikawa [3], Manika Dhanasekar [4], and Les Dawes [4]

ABSTRACT

Cumulative plastic deformation characteristics of rail tracks under moving wheel loads are complex problems. Globally the rail industry is challenged by effective maintenance strategies to ensure safety of the rail track structures. Influence of particle size distributions (PSDs) on the cyclic cumulative plastic deformation of coarse materials in the rail track substructure layers under moving wheel load is not well understood. Conventional test approaches, namely the direct shear test, the cyclic single point load test, and the California bearing ratio test, cannot replicate the actual stress-strain state of coarse materials under moving wheel loads. The multi-ring shear apparatus, an improved torsional simple shear apparatus to replicate moving train wheel loading conditions, was used in this study. The PSDs of coarse materials were experimentally simulated through modifications to the mass portions of different glass beads. The moving wheel loads introduce higher plastic deformation and lower resilient modulus irrespective of the PSDs compared to cyclic single point load tests. Further study with three natural coarse materials (Toyoura sand and two ballast types) indicates that the cumulative plastic deformation has nonlinear relationships between the principal stress axis rotation and PSDs of the materials.

Key words: Particle size distribution, cumulative plastic deformation, multi-ring shear apparatus, moving wheel load, glass bead.

1. INTRODUCTION

Cumulative cyclic plastic settlement of the rail track substructure layers is a significant problem in the rail industry. This leads to expensive maintenance cycles for ensuring passenger comfort and safety and also minimising speed restrictions. The cumulative cyclic plastic settlement depends on the loading amplitude, frequency, number of cycles, material physical state, substructure layer thickness, and weather (Li and Selig 1994; 1996; Li and Selig 1995; Hesse *et al.* 2014; Li *et al.* 2015). Current guidelines do not consider the cumulative plastic settlement in the rail track design, including the transition zone (Burrow *et al.* 2007; Dareeju *et al.* 2014). However, Li and Selig (1998a; 1998b) accounted for the effects of the cumulative tonnage as a function of the cumulative cyclic plastic settlement of the rail track substructure. Analysing the field observations in British rail tracks, Burrow *et al.* (2011) further showed the significance of the cumulative tonnage in determining the ballast layer thickness to minimise the excessive settlement. Besides these factors, particle size distribution (PSD), fabric, stress history, and the confinement of materials, can also control the rate of cumulative cyclic plastic settlement of the rail tracks (Li *et al.* 2015).

Influence of PSDs of the coarse materials on the cyclic plastic deformation was examined using conventional experimental methods such as the cyclic triaxial and cyclic direct shear tests (Indraratna *et al.* 2003; Indraratna *et al.* 2004; Momoya *et al.* 2005). The results indicated that the well-graded coarse materials show the least plastic settlement, followed by gap-graded materials than the uniform materials. The principal stress axis rotation (PSAR), a result of changing stress state of a given element by the location of the moving wheel, is unable to be replicated by these conventional testing methods. PSAR can influence both resilient and residual deformation characteristics of substructure materials at any saturation stage (dry, unsaturated, or saturated) (Indraratna *et al.* 1998; Lekarp *et al.* 2000; Powrie *et al.* 2007; Gräbe and Clayton 2009; Ishikawa *et al.* 2015; Gallage *et al.* 2016; Dareeju *et al.* 2017). Furthermore, the recent studies suggested that the response (stress-strain) of the track substructure under the PSAR is significantly different with the single point load (conventional triaxial test) (Anderson and Key 2000; Hirakawa *et al.* 2002; Momoya *et al.* 2005; Powrie *et al.* 2007; Gräbe and Clayton 2009; Ishikawa *et al.* 2011). The cyclic plastic deformation governed by the PSAR, however, still associates with a number of uncertainties in spite of several studies (Gräbe and Clayton 2009; Yang *et al.* 2009; Ishikawa *et al.* 2011).

Compositional and structural changes of coarse materials can lead to stiffening, softening, or altered hydraulic conductivity properties even under similar packing indices. Previous studies (Hirakawa *et al.* 2002; Momoya *et al.* 2005; Ishikawa *et al.* 2011) neglected such changes in evaluating the cyclic plastic deformation of coarse materials with/without the PSAR effects. Therefore, the

Manuscript received December 2, 2016; revised February 8, 2018; accepted June 25, 2018.
[1] Ph.D. Scholar, Science and Engineering Faculty, Queensland University of Technology (QUT), 2 George St., Brisbane, QLD 4000, Australia.
[2*] Senior Lecturer (corresponding author), Science and Engineering Faculty, Queensland University of Technology (QUT), 2 George St., Brisbane, QLD 4000, Australia (e-mail: chaminda.gallage@qut.edu.au).
[3] Professor, Faculty of Engineering, Hokkaido University, Kita13, Nishi8, Kita-ku, Sapporo, Hokkaido, 060-8628, Japan.
[4] Professor, Science and Engineering Faculty, Queensland University of Technology (QUT), 2 George St., Brisbane, QLD 4000, Australia.

deformation characteristics of coarse materials with known PSDs were examined in this study using composite materials and their performance was further validated using three different, natural material types under the similar loading conditions.

2. TEST METHOD

2.1 Test Apparatus

Figure 1 illustrates the schematic diagram of the multi-ring shear (MRS) apparatus used in this study. The apparatus accommodates a hollow cylindrical material specimen with 100 mm height, 120 mm inner diameter, and 240 mm outer diameter. The inner and outer cylindrical surfaces of the specimen are confined by rigid rings as shown in Fig. 1. The height of each ring is 20mm. Both vertical axial stress (σ_a) and torsional shear stress ($\tau_{a\theta}$) are introduced by a direct drive motor. Readings of the load cell mounted on loading plate and torque transducer located under the bottom plate are used to calculate axial stress and shear stress, respectively. Axial deformation to calculate axial strain (ε_a) of specimen is measured by an external LVDT. Using the rotational angle of the direct drive motor, shear strain ($\gamma_{a\theta}$) of the specimen is estimated. A detailed description of this multi-ring shear apparatus and its applications are available in Ishikawa *et al.* (2011) and Inam *et al.* (2012). Due to zero circumferential strain (ε_θ) and radial strain (ε_r), axial strain is equal to volumetric strain (ε_v) of specimen under any loading condition.

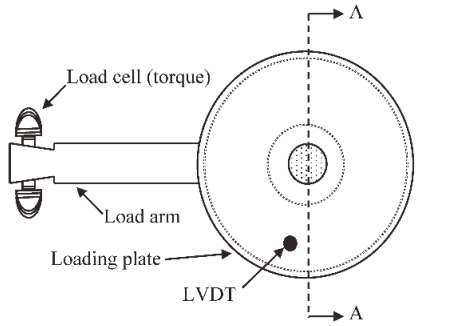

(a) Plan-view

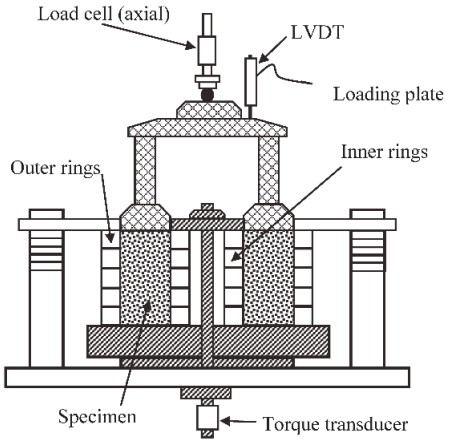

(b) Cross-section

Fig. 1 Schematic diagram of modified multi-ring shear apparatus

2.2 Materials Used

Two different spherical glass bead particles: 2.5mm and 5mm diameters were used in this study. Glass beads are typically used as a type of transparent material particles in geotechnical laboratory modelling (Ishikawa *et al.* 2011; Likos and Jaafar 2013). The specific gravity of glass beads is 2.56 in accordance with ASTM D854 (2014). Due to lower water absorption properties of the glass beads, only air-dried glass beads were used in this study. Table 1 summarises the composition of the five composite material types (A, B, C, D, and E) chosen in this study.

Table 1 Mixing percentages of glass beads to produce different material types

Material name	Percentage of 5mm glass beads (%)	Percentage of 2.5mm glass beads (%)
Type A	100	00
Type B	75	25
Type C	50	50
Type D	25	75
Type E	00	100

Three natural materials: Two types of ballast materials and Toyoura sand were further studied to investigate the influence of material PSDs on the deformation properties of coarse materials. Toyoura sand is commercially available material and ballast types used in this study are within the range of lower and upper limit of Japanese standard ballast gradation and commonly used in the model tests (Kumara and Hayano 2016). Table 2 and Fig. 2 show the basic properties of these materials and the grain-size distribution of Toyoura sand, Ballast 2, and Ballast 1 obtained from dry sieving in accordance with ASTM D422-63 (2007).

Table 2 Basic parameters of actual materials

Test material	D_{50} (mm)	D_{max} (mm)	ρ_{max} (g/cm^3)	ρ_{min} (g/cm^3)
Ballast 1	8.1	12	1.65	1.35
Ballast 2	6.2	12	1.70	1.39
Toyoura sand	0.17	0.6	1.64	1.34

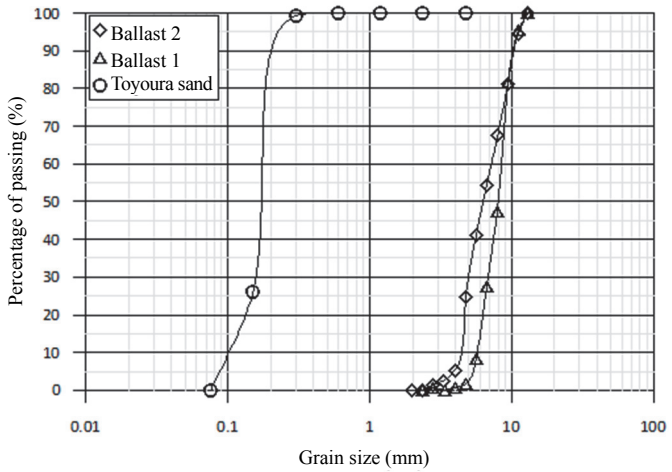

Fig. 2 Particle size distributions of natural materials used

2.3 Sample Preparation

In sample preparation, setting a packing indices, dry density, relative compaction (*RC*), or relative density (D_r), was proposed. However, the estimated density values (maximum and minimum densities) of the composite material types, using JIS A 1224-2009 were unreliable due to rounded shape of the particles and the limitation of the standard. JIS A 1224-2009 is designed only for sand materials and, therefore, material types C, D and E can be classified as sand materials. As estimated relative densities were unreliable, constant dry density and relative compaction were possible packing indices for the sample preparation. The lower water absorption property of glass beads is the key drawback in finding maximum dry density and optimum water content. Due to lower water absorption properties of glass beads, only air-dried samples can be prepared. It was therefore difficult to maintain constant relative compacted samples. From the available options, particle density ratio (dry density/particle density) was selected as a packing index, as it only depends on the void ratio of the specimen.

After a series of trial and error experiments, the initial and target dry densities for the sample preparation were selected as 1.58 g/cm^3 and 1.62 g/cm^3, respectively, with a tolerance of ±0.001 g/cm^3. As natural materials do not comply with above complications, 85% of the maximum dry density was selected as the packing index, where the target dry densities of Toyoura sand, Ballast 1, and Ballast 2, were 1.39 g/cm^3, 1.4 g/cm^3, and 1.45 g/cm^3, respectively. In the initial sample preparation, the dry density was compacted to achieve 80% of the maximum dry density. However, applying pre-loading cycles to obtain target stresses in the MRS tests is required, after achieving the target dry density. These pre-loading cycles caused an initial settlement, resulting in altered dry densities. A trial and error study indicated that these alterations of the dry density were not uniform, and a constant compacted (consolidated) dry density was difficult to achieve. Previous studies agree with this observation, where initial settlement of coarse materials under the PSAR during the pre-loading cycles are significantly higher, compared to the similar samples subjected to single point loading (without the PSAR effects) even at elastic shakedown limits (Gallage *et al.* 2016; Dareeju *et al.* 2017). Therefore, this study did not control the final density after pre-loading cycles.

To prepare the samples, the MRS apparatus was set up with inner and outer rings as illustrated in Fig. 1, and then materials were poured into the space formed by these rings using three equally thick layers. A cone was used in this step to minimise the particle segregation. Each material layer was compacted by tamping with a wooden hammer until initial dry density was achieved. As energy applying through tamping is difficult to maintain, this initial density was defined. Furthermore, the height (thickness) of the sample indicated the density of the specimen in tamping. To obtain the target dry density, a static vertical (axial) load was applied with a constant rate of 0.1 %/min until the pre-determined sample height was reached. Note that the initial deformation by the self-weight of loading plate was neglected in this study due to unavailability of a measuring method. The prepared specimens were tested under static shear, cyclic single point (without PSAR), and cyclic moving wheel (with PSAR) loading conditions.

2.4 Loading Conditions and Load Application

Ishikawa *et al.* (2011) observed axial stress of 80 kPa and shear stress of 12.8 kPa on the ballast layer under 2 kN vertical train load with a constant 700 mm/min speed, using one-fifth scaled model tests of the traditional Japanese rail tracks. Otter (2011) further agreed with these observations, indicating the effective stresses applied on the rail foundation substructure lies between 10 kPa and 400 kPa. As illustrated in Table 3, a series of MRS tests were conducted on both composite and natural material types, adopting the stress state from Ishikawa *et al.* (2011).

Table 3 Loading conditions used

Loading method	Axial stress, σ_a (kPa)	Shear Stress/Strain	Number of loading cycles (N_c)	Loading frequency (Hz)
Static shear	80	0.1%/min	--	--
Cyclic single point	80	0 kPa	200	0.017
Cyclic moving wheel	80	12.8 kPa	200	0.017

To replicate static direct shear testing conditions, torsional static shear test series was performed under a constant axial stress of 80 kPa and shear strain rate of 0.1 %/min. The applied axial stress was achieved using eight equal axial stress increments under axial stress-controlled method. Figure 3(a) shows the loading conditions of the torsional static shear test. In this study, cyclic single point load test was implemented to replicate the stress state of the conventional cyclic triaxial compression testing conditions. The axial stress with amplitude of 80 kPa was introduced in a half sinusoidal waveform with zero shear stress as given in Fig. 3(b). Raymond and Davies (1978) claimed that sinusoidal waveform is the most suitable loading pattern to replicate the actual loading history under a sleeper, produced by a moving wheel load.

The loading conditions used in cyclic single point load test were unable to replicate the moving wheel load conditions (no PSAR) and only represent the stress state of a point, when the wheel is exactly above the point. Therefore, to simulate cyclic moving wheel load, both axial stress with an amplitude of 80 kPa in half-sinusoidal waveform and shear stress with an amplitude of 12.8 kPa in sinusoidal waveform were simultaneously applied as illustrated in Fig. 3(c). Changing the phase angle of shear stress by 180° for each succeeding cycle, two-way moving wheel load was simulated as explained by Inam *et al.* (2012) and Dareeju *et al.* (2016). Introduction of shear stress in to the cyclic single point load conditions can produce the PSAR on coarse materials. Therefore, the effects of PSAR on the deformation characteristics of the coarse materials are discussed in this study with the comparison between cyclic single point load test and cyclic moving wheel load test.

Eight pre-loading cycles were used to achieve the target amplitudes of both cyclic tests in this study as illustrated in Fig. 4. Then, 200 loading cycles with a loading frequency of 0.017 Hz were applied to the samples. Dareeju *et al.* (2017) proved that low frequency can introduce higher plastic deformation under the PSAR given that dynamic effects are insignificant. This study therefore adopted this low frequency. Since previous studies agreed with this observation (Inam *et al.* 2012; Ishikawa and Miura 2015), this study did not investigate the combined effects of loading frequency and material PSDs on the deformation properties. During loading, axial stress (σ_a), axial strain (ε_a), torsional stress ($\tau_{a\theta}$), and shear strain ($\gamma_{a\theta}$) were calculated and recorded every second.

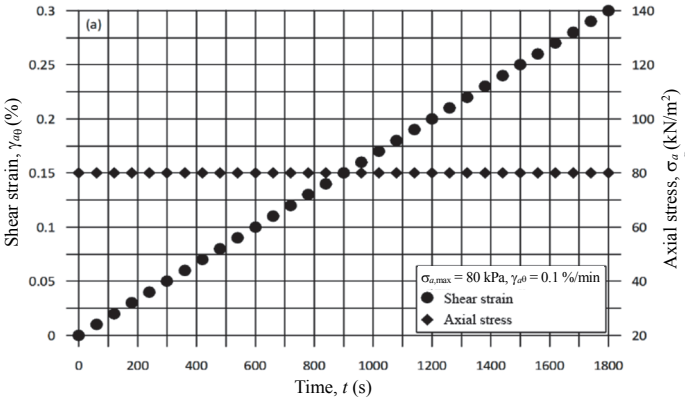

(a) Static torsional shear

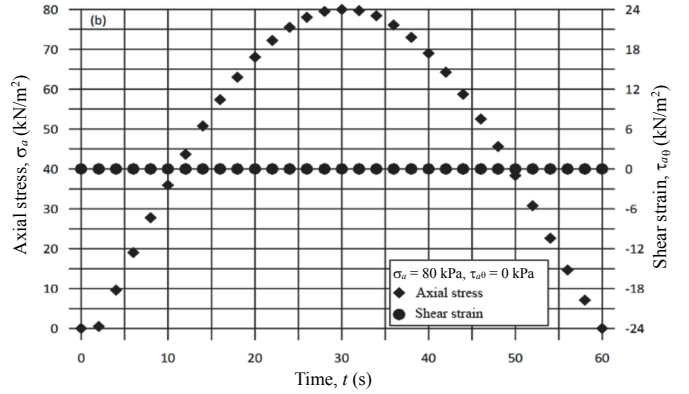

(b) Single point load

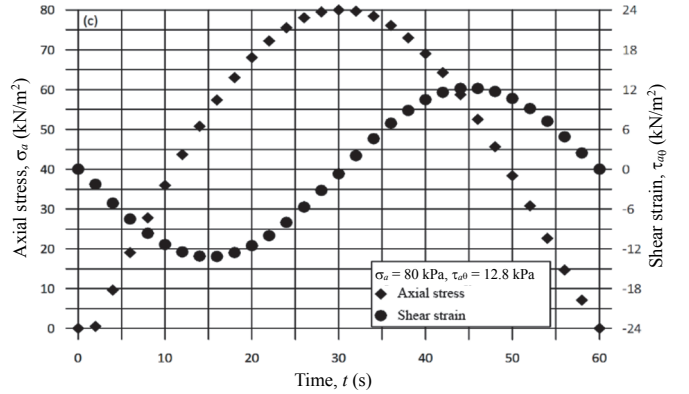

(c) Moving wheel load

Fig. 3 Loading conditions used

3. RESULTS AND DISCUSSIONS

3.1 Effects of PSDs on Shear Behaviour of Coarse Materials

Figure 5 illustrates the shear stress – shear strain relationships of the composite material types. To eliminate the effects of pre-loading cycles, all values were initialised. All material types exhibit non-linear shear shress-strain behaviour, which is similar to the typical response of coarse materials under static direct shear tests. Shear stress increases with increasing shear stress irrespective to the PSDs. Presence of higher precentage of 2.5 mm particles in materials can enhance both shear resistance and shear modulus up to 1% shear strain as shown in Fig. 5. However, further increases of shear strain produce an optimum mix ratio of material particles (75% of 2.5 mm + 25% of 5 mm—material type D) in regard to maximum shear shear resistance and shear

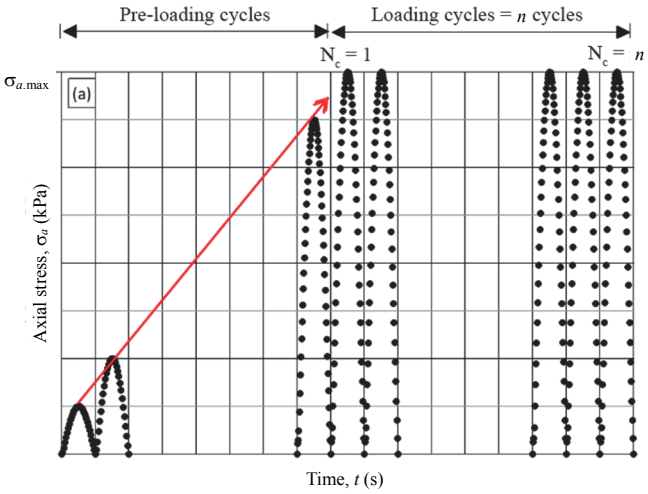

(a) Single point load

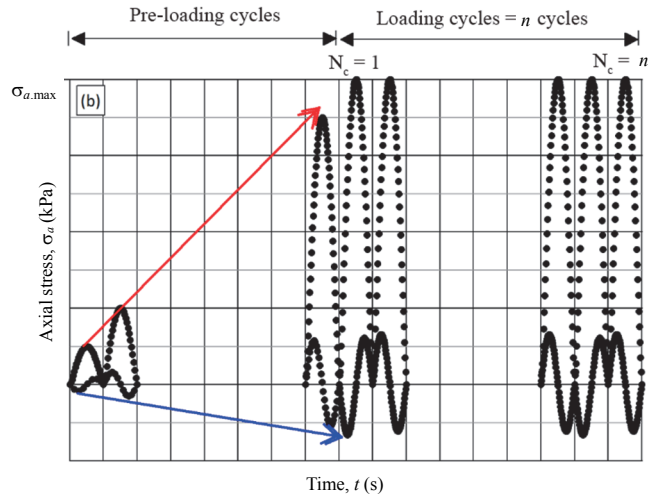

(b) Moving wheel load

Fig. 4 Stress state of cyclic loadings

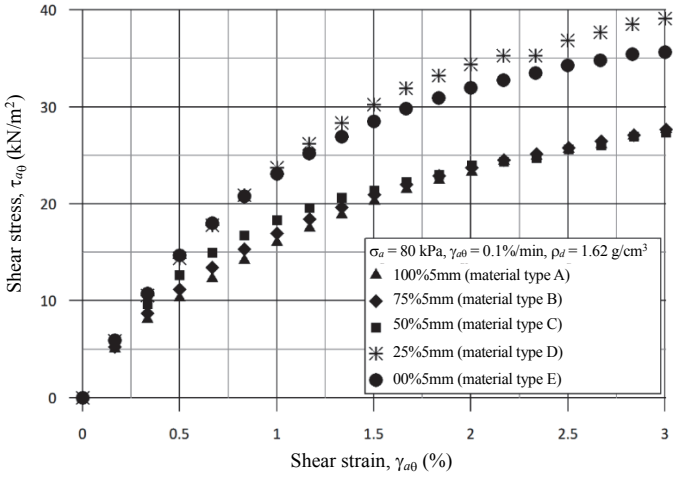

Fig. 5 Shear stress – shear strain relationships of constituted soils

modulus. Higher precentage of surface contact area by the smaller particles can interlock the particles, introducing a higher shear resistance to the particle movements. It is clear that gap-graded materials can be highly shear-resistant compared to uniformly graded material. However, according to Holtz and Kovacs (1981), the peak shear stress of samples with an identical void ratio is a

constant, and there is no influence from the PSD of the material. Material types A, B, and C agree with this observation and the material with higher percentage of small particles is altered, even having a constant initial void ratio. However, Holtz and Kovacs (1981) further argued that the change of the angularity can alter the peak shear stress even under a constant packing index. Since all composite materials have a similar angularity and a constant void ratio, the altered shear capacities of material types D and E are the result of pre-loading increments. To compare results between static shear and cyclic loadings (single point and moving wheel), similar pre-loading steps were maintained in this study. Therefore, a constant final density (consolidated) was unable to be ensured and pre-loadings may have densified these two material types, resulting in a relatively high shear strength. Dafalla (2013) however showed that change of the clay percentage of clayey sand mixtures with a constant packing index (relative density) can alter the shear strength of material using static direct shear test. The peak shear stresses of materials with increasing clay precentage under low water contents and maximum shear stresses of the air-dried composite materials in this study with increasing 2.5 mm particles illustrate a similar behvaiour. Therefore, further investigation is required to quantify the performance of finer materials on the shear.

Figure 6 shows the the relationships between shear strain – axial strain of the composite material types to observe the volume change behaviour of materials during shearing: positive axial strain means contraction (volume decrease) and negative axial strain means dilation (volume increase). Materials with higher precentage of 5 mm particles contact show increasing shear strain, while the ones with higher 2.5 mm particles dilates. Even having a constant inital void ratio, material types A, B, and C (materials with low interpaticle surface contact area) illustrate loose behaviour and the rest, materials with higher interparticle surface contact area have dense properties. Bolton (1986) further showed that dilation only depends on the relative density, when the particle crushing is not possible and other factors such as loading rate, material water content, and axial load are constant. As it is not possible to break the particle used for composite material preparation, a slight change of initial void ratio at the end of pre-loading steps can also be a possible reason behind these altered dilations or contraction. However, it indicates that there is no significant variation of axial strain between material types

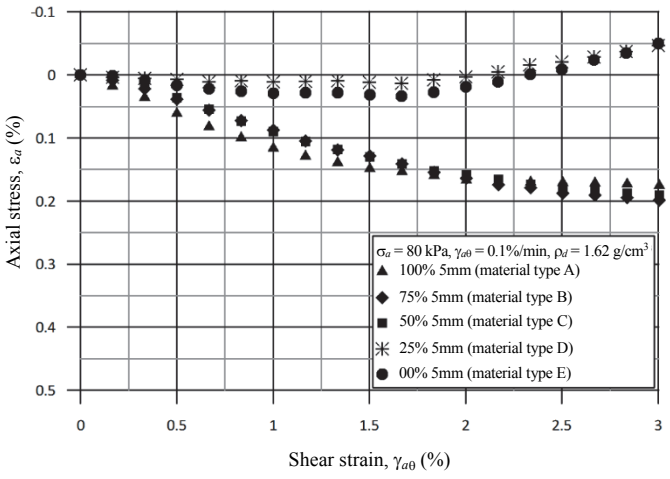

Fig. 6 Axial strain – shear strain relationships of constituted soils

within each group: loose or dense as shown in Fig. 6. The restriction of shear strain to a maximum of 3% due to the limitation of the apparatus can be the possible reason behind this performance.

Figure 7 summaries the effects of material PSD on shear strain and axial strain relationship at shear stress of 12.8 kPa and 25.6 kPa under static torsional shearing. For this comparison, two shear stresses were selected, considering the amplitude of shear stress of cyclic moving loading test as the fundamental limit. Increasing percentage of 2.5 mm particles decreases both shear strain and axial strain irrespective to the shear stress. The reduction of both shear and axial strain at a lower stress level is insignificant with respect to the particle size as shown in Fig. 7. According to Figs. 6 and 7, at higher stress levels, both shear and axial strains of material types D and E are considerably reduced compared to other material types as a possible result of the pre-loading increments.

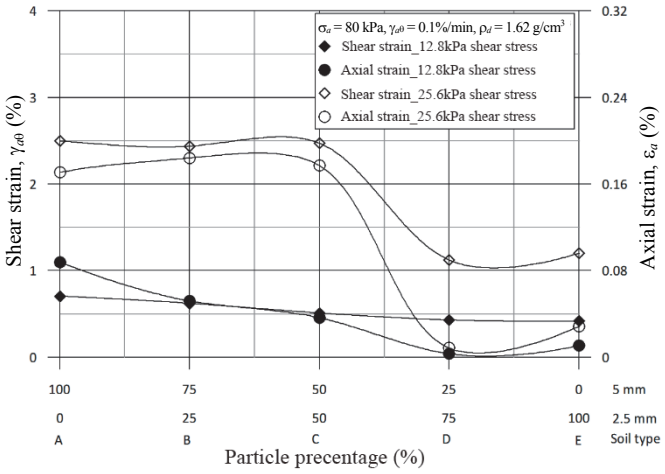

Fig. 7 Shear strain – axial strain – PSD relationships of constituted soils

3.2 Effects of PSDs on Cyclic Plastic Deformation of Coarse Materials

Figure 8 illustrates the axial stress – axial strain relationships of material type A under different cyclic load conditions. Progressive reduction of the area of hysteresis loops with loading cycle number indicates that the specimens gained more resilient properties (elastic) with loading cycle number irrespective of the loading method. This observation further highlights that the specimens were subjected to higher plastic deformation at the early stages of loading regardless of the loading method. A similar observation in coarse-grained materials: ballast and sub-base materials under similar loading methods was highlighted by Ishikawa *et al.* (2011), Inam *et al.* (2012), and Ishikawa and Miura (2015). The strain amplitude, the difference between the maximum and plastic strain, gradually increases within early loading cycles and then becomes a constant with loading cycle number. Therefore, the maximum axial strain can be used as an indicator of accumulation of plastic deformation in cyclic loading tests. These observations illustrate the higher irreversible deformation experienced by the new/fresh maintained rail tracks at its early stage. As shown in Fig. 8, the area of hysteresis loops of the samples subjected to cyclic moving wheel load is significantly large, compared with cyclic single point load. Furthermore, the

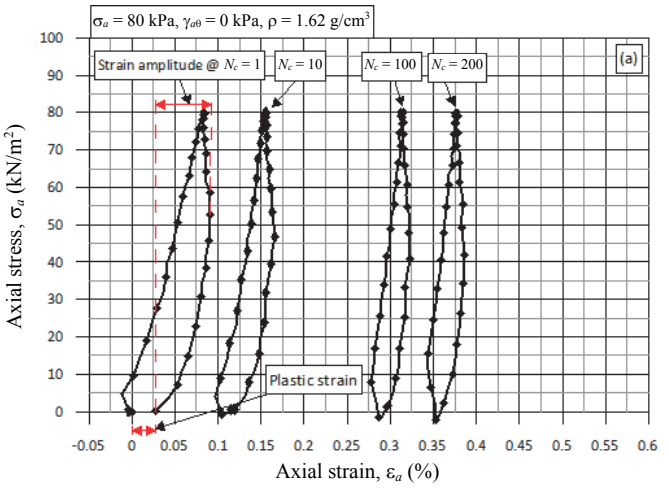

(a) Cyclic single point loading

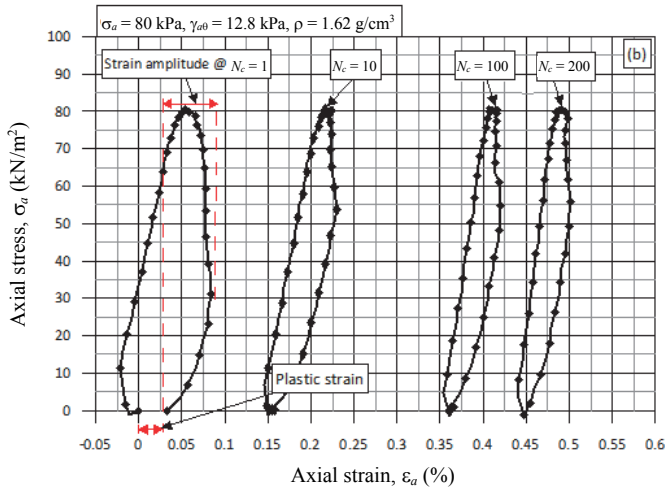

(b) Cyclic moving wheel loading

Fig. 8 Axial stress – axial strain relationship of material type A

cyclic moving wheel load produces higher accumulation rate of the strain amplitude, reaching its shakedown limits promptly before cyclic single point load. This behaviour indicates that the PSAR can produce a higher plastic deformation and reach the material shakedown limits quickly.

Figure 9 shows the cumulative plastic strain – number of loading cycle relationships of the composite material types under cyclic single point loading conditions. Irrespective of the material type, the plastic strain increases with increasing loading cycles. The accumulation rates of the plastic strain of all samples are significantly high during first 25 loading cycles, and then they gradually diminish with increasing loading cycles. Pre-stabilisation of rail substructural materials can result in a higher irreversible deformation at the early stage of the service life. The rate of this progressive stabilisation decreases with time, introducing advanced resilient properties into the track as shown in Figs. 8 and 9. This phenomenon can be further validated, using the previous field and laboratory test results (Hirakawa *et al.* 2002; Momoya *et al.* 2005; Gräbe and Clayton 2009; Ishikawa *et al.* 2011; Shahin *et al.* 2011; Loh and Nikraz 2012). The gap graded materials excluding material type D were subjected to a higher cumulative plastic deformation, compared to the uniformly graded materials after 25 loading cycles. Material type C, a gap graded material, furthermore has the maximum cumulative plastic

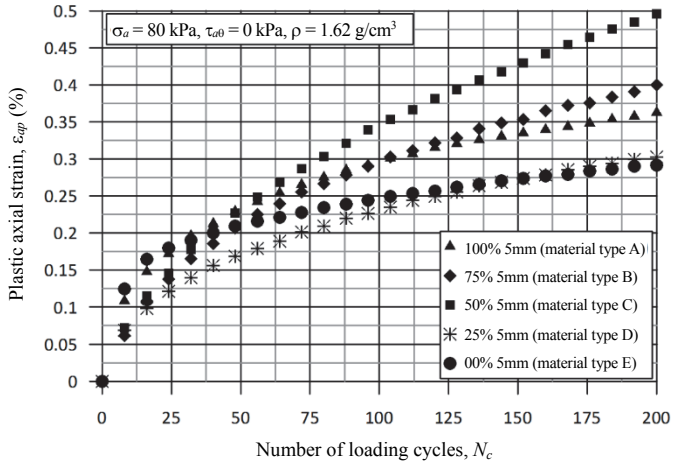

Fig. 9 Plastic axial strain – number of loading cycles relationships of constituted soils under cyclic single point loadings

strain. During this early loading stage, the uniformly graded material has higher cumulative plastic deformations. This indicates that the pre-stabilization at the early loading cycles is more dominant in uniformly graded materials. The absence of other particle sizes significantly discourages the particle rearrangement in uniformly graded materials. This may be the possible reason that demonstrates higher cumulative plastic deformations in gap graded materials, after the early loading cycles. Indraratna *et al.* (2003) however showed that uniform materials with highest average breaking index display the maximum plastic deformation, while moderately graded materials have the least. These observations highlight that gap graded materials tend to experience higher irreversible deformation, compared to the uniformly graded materials with negligible material breaking indices.

Figure 10 outlines the cumulative plastic strain – loading cycle relationships of three natural coarse grained material types (Ballast 1, Ballast 2, and Toyoura sand) under cyclic single point loading conditions. Similar to the response of the composite materials, the cumulative plastic deformation increases with increasing loading cycles irrespective of the material type. According to Figs. 9 and 10, the accumulation rates of plastic strain of natural materials also have an identical performance with the composite materials. As shown in Fig. 10, Toyoura sand has the lowest cumulative plastic strain irrespective to loading cycle number. Toyoura sand is however expected to have the highest cumulative plastic deformation, considering its minimal D_{max} (maximum particle size) among these three materials. Generally, the shear resistance of material is directly proportional to the maximum particle size under static direct shear testing conditions. However, according to Indraratna *et al.* (2016), the peak friction angle of ballast materials has a non-linear relationship with coefficient of uniformity (C_u). Under either constant void ratio or relative density, the ballast materials contain a maximum peak friction angle and a corresponding optimum coefficient uniformity. According to their observations, the optimum coefficient of uniformity of ballast materials is approximately equal to 2.5. The performance of Toyoura sand (C_u = 1.58) and two ballast materials (1/5A: C_u = 1.52 and 1/5B: C_u = 1.55) under cyclic single point loading conditions aligned with these observations. Ishikawa *et al.* (2011) experienced a similar response in ballast materials under cyclic loading conditions.

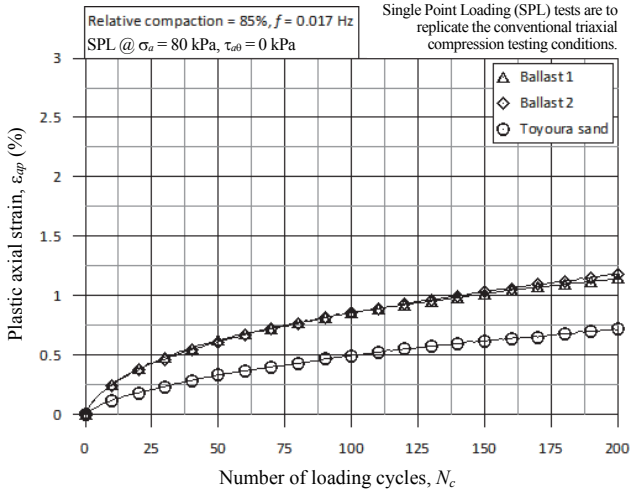

Fig. 10 Plastic axial strain – number of loading cycles relationships of natural soils under cyclic single point loading

Figures 11 and 12 illustrate the relationships between the cumulative plastic strain of both the composite and natural materials and loading cycles, respectively, under cyclic moving load. The results of cyclic moving wheel loading tests (with effects of PSAR) are similar to cyclic single point loading tests, showing increasing cumulative plastic deformations with increasing loading cycles. The cumulative plastic deformation of all tested material types under moving wheel loading conditions is much higher than those caused by cyclic single point loading conditions irrespective of the material type and loading cycle number. Since having identical PSDs and insignificant ability of particle breaking or self-deforming, this considerable influence on the cyclic cumulative plastic deformation of coarse grained materials is a result of the presence of the PSAR in the cyclic moving wheel loading tests. As shown in Fig. 11, the gap graded materials has the more cumulative plastic deformation than the uniformly graded materials under the effects of the PSAR. The relationships of cumulative plastic deformation and the coefficient of uniformity of coarse grained natural materials, explained under cyclic single point loading conditions, are still valid even with cyclic moving wheel loading conditions as illustrated in Fig. 12.

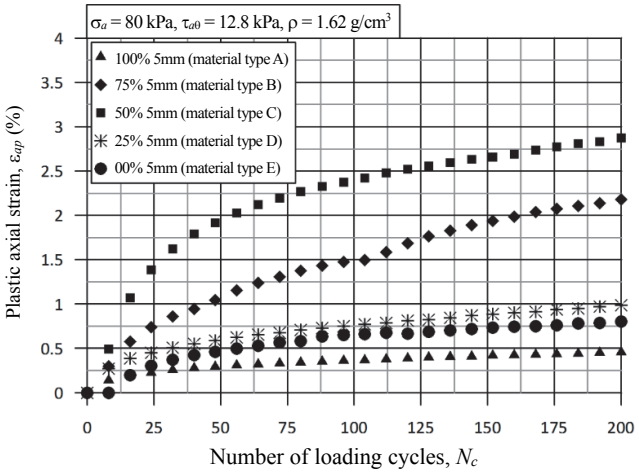

Fig. 11 Plastic axial strain – number of loading cycles relationships of constituted soils under cyclic moving wheel loadings

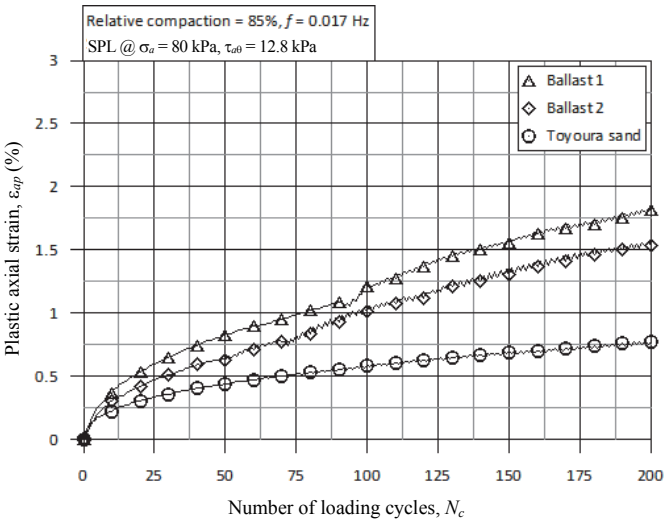

Fig. 12 Plastic axial strain – number of loading cycles relationships of natural soils under cyclic moving wheel loading

3.3 Correlations of PSDs and PSAR on Cyclic Deformation Characteristics of Coarse Materials

Figure 13 shows the cumulative plastic strain at 100th loading cycle – normalised particle size ratio relationships of both the composite and natural materials under cyclic single point loading and cyclic moving wheel loading test conditions. Only binary particle size mixtures is used for the preparation of the composite materials and the use of maximum (D_{max}) or mean (D_{50}) particle size for the comparison is inadequate. Therefore, this study developed a normalised particle ratio by dividing mean particle size by maximum particle size. Having the same particle size distribution, density, and water content, the presence of effects of the PSAR in the cyclic moving wheel loading tests is the only reason to increase plastic deformation of coarse materials irrespective of the material type as shown in Fig. 13. Furthermore, under the magnitudes of the applied stress and loading cycles, the effects of particle breakage and particle self-deformation can be neglected. The plastic deformation of the composite materials, from material A to material E, increased by 22%, 410%, 594%, 227%, and 161%, respectively, after introducing the PSAR into the cyclic single point loading tests. These observations indicate that gap graded materials are more vulnerable to irreversibly deform with the effects of the PSAR than the uniformly graded materials. Furthermore, the plastic deformation of Ballast 1, Ballast 2, and Toyoura sand influence are amplified by 44%, 21%, and 19%, respectively, compared to the samples without the PSAR influence. The plastic deformation increments of the natural materials followed the correlations between the coefficient of uniformity and the plastic deformation of materials with and without the PSAR. Since the relationships of the PSDs of the materials and the PSAR can non-linearly introduce higher plastic deformation properties, the current design guidelines and parameters should be carefully re-examined to include the effects of the PSAR. As the current guidelines/design equations are mainly based on cyclic triaxial tests, the permanent deformation characteristics are therefore underestimated due to the absence of the PSAR. This supposition further highlights that two different deformation mechanisms are dominant in each cyclic test conditions. The

deformation of the samples under cyclic single point loading conditions is controlled by the compression due to zero shear component. The shear deformation is more significant in the samples with the PSAR. Using three different amplitudes of shear stress, including zero, Inam *et al.* (2012) showed that the cyclic plastic deformation increases with increasing shear stress under a constant amplitude of the normal stress.

The rate of axial strain, which was estimated as the ratio of the cumulative plastic deformations between under cyclic moving wheel loading (with PSAR) and cyclic single point loading (without PSAR), is an indicator to measure the effects of the PSAR on both resilient and residual deformation properties (Gräbe and Clayton 2009; 2014; Ishikawa *et al.* 2011; Ishikawa and Miura 2015). Since this study focuses on the residual deformation characteristics, the rate of axial strain was calculated using the cumulative plastic deformation. Ishikawa *et al.* (2011) and Dareeju *et al.* (2017) showed that the rate of axial strain is approximately constant irrespective of the loading cycle number; however, it depends on loading method, dry density of soil, and material type. The rate of axial strain calculated for each soil type in this study also agrees with above observations. Figure 14 illustrates the rate of axial strain – normalised particle size ratio relationships of both the composite and natural materials at 100 loading cycles. The rate of axial strain of gap graded materials is considerably higher than the uniformly graded soil. This behaviour highlights that gap graded materials can be subjected to higher plastic deformation with the PSAR effects if material breakage or self-deformation is not possible. As explained in Fig. 10, the cumulative plastic deformations of the natural materials have a nonlinear relationship with the cofficient of uniformity. The ratio of axial strain of the natural soil has this identical nonlinear relationship with the cofficient of uniformity, where Toyoura sand has the least ratio of axial strain, while Ballast 1 has the highest. Gräbe and Clayton (2009) further proved that decreasing the percentage of clay in materials can nonlinearly increase the rate of axial strain. The performance of the ratio of axial strain in this study agree with observed relationship between the peak friction angle and the the cofficient of uniformity of coarse materials by Indraratna *et al.* (2016) and Gräbe and Clayton (2009). These results therefore indicate that the PSAR effect on the deformation characteristics of coarse materials is a function of the coefficient of uniformity.

A realistic evaluation of the resilient performance of the substructure materials is essential in designing rail tracks. The resilient modulus is the common basis to evaluate the resilient behaviour of substructure materials. Figure 15 shows the strain amplitude (resilient deformation) – normalised particle size ratio relationships of all material types at 100 loading cycles. The strain amplitude is a direct indicator of the resilient modulus, where it can be calculated by dividing the amplitude of the normal stress by the strain amplitude. The amplitudes of both cyclic single point loading and cyclic moving wheel loading tests are constant. As shown in Fig. 16, the PSAR can reduce the resilient modulus of any coarse materials due to higher strain amplitudes gained under cyclic moving wheel loading conditions. Gräbe and Clayton (2014) and Dareeju *et al.* (2017) also highlighted the similar performance of soils with the effects of the PSAR. As shown in Fig. 15, gap graded materials (material types B, C, and D) have the least resilient modulus irrespective of the loading method. Gräbe and Clayton (2014) found that the

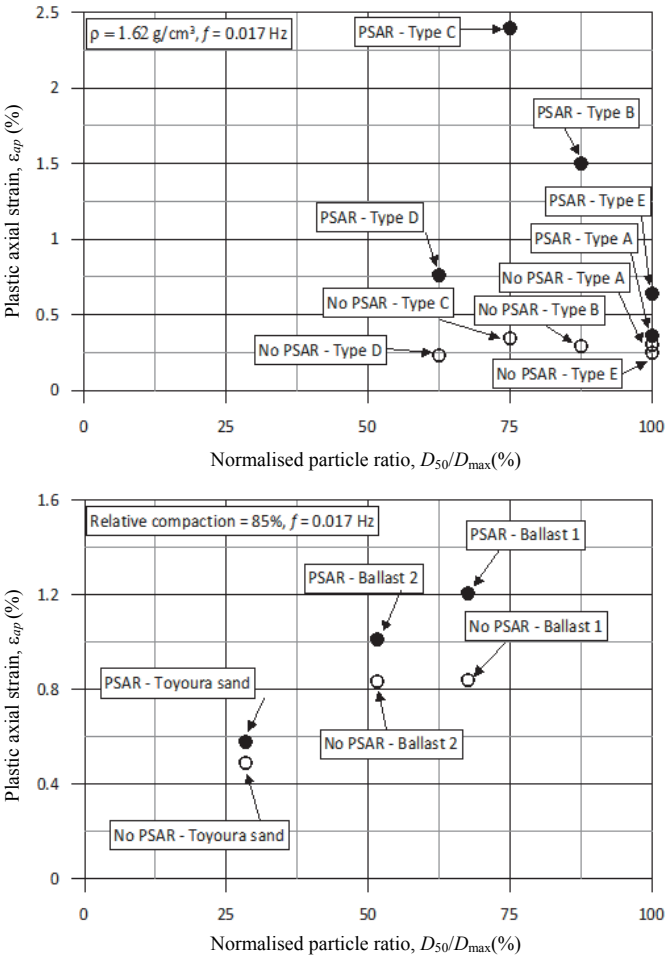

Fig. 13 Effects of PSAR on plastic axial strains of soils

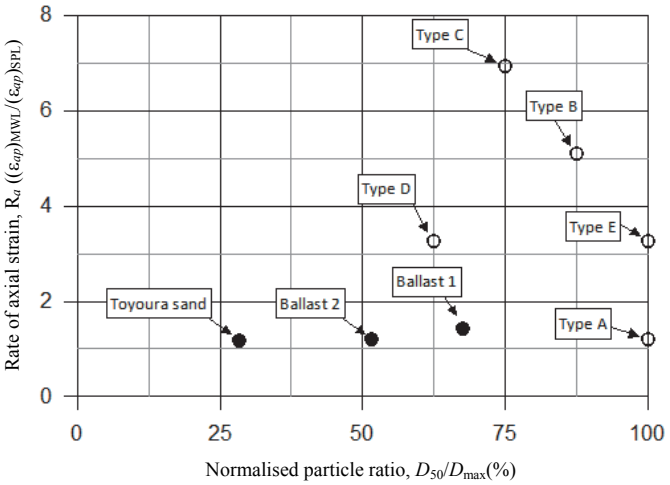

Fig. 14 Effects of PSAR on rate of axial strains of soils

resilient modulus of soil materials have an optimum coefficient of uniformity under any cyclic loading conditions. The results of this study indicate a similar trend in the coarse materials with and without PSAR. It is clear that the different performance between with and without PSAR in Figs. 13 to 15 is a result of the dilation effects of granular soils subjected to shear loading. Inam *et al.* (2012) and Ishikawa and Miura (2015) also agreed with this

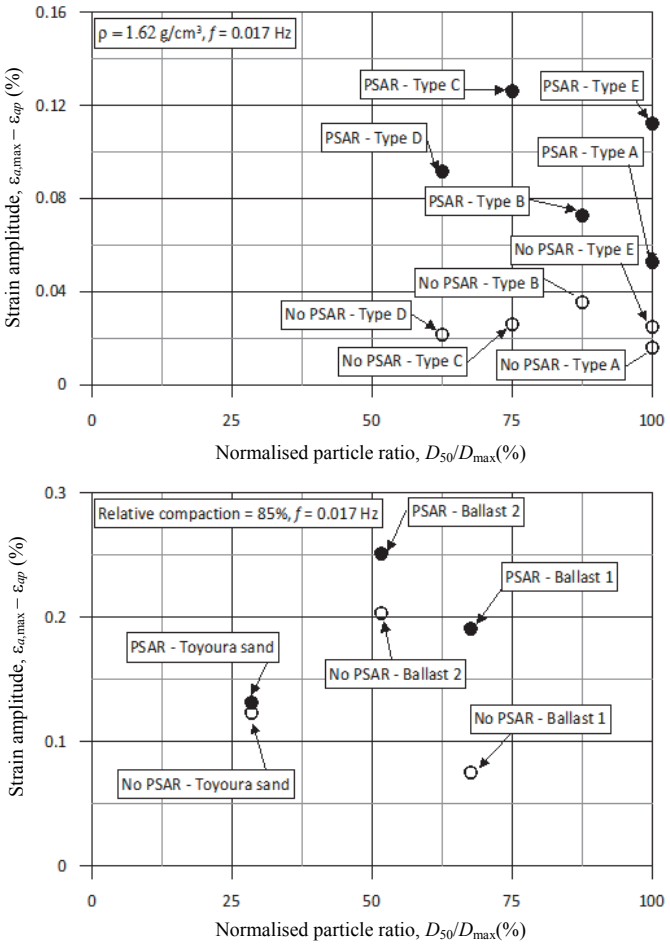

Fig. 15 Effects of PSAR on strain amplitude of soils

observation. The results showed that higher shear stress can increase the parameters highlighted in Figs. 13 to 15 if normal stress and initial void ratio are constant.

CONCLUSIONS

The following conclusions are derived from the research study described in this paper:

1. Both static torsional shear and cyclic single point loading tests underestimate the plastic deformation characteristics of any materials types (regardless of PSDs) compared to cyclic moving wheel loading tests (with PSAR). Therefore, the current design guidelines, which are unable to account the PSAR, are needed to re-examine.
2. PSAR introduces a higher cumulative plastic deformation in gap graded coarse materials than uniformly graded materials. This indicates that the PSAR is more dominant in gap graded materials.
3. PSAR can reduce the resilient modulus of any material types (regardless of PSDs) compared with cyclic single point loading tests.
4. PSAR has nonlinear relationships with the coefficient of uniformity of coarse materials on plastic deformation and resilient modulus. These nonlinear relationships can be used to define a PSD, which has the minimum influence by the PSAR.

REFERENCES

Anderson, W. and Key, A. (2000). "Model testing of two-layer railway track ballast." *Journal of Geotechnical and Geoenvironmental Engineering*, ASCE, **126**(4), 317-323. https://doi.org/10.1061/(ASCE)1090-0241(2000)126:4(317)

ASTM D422-63 (2007). *Standard Test Method for Particle-Size Analysis of Materials*, ASTM Internatinal, West Conshohocken, PA2007. https://doi.org/10.1007/978-0-387-30160-0_837

ASTM D6913-04(2009)e1 (2009). *Standard Test Methods for Particle-Size Distribution (Gradation) of Materials Using Sieve Analysis*, ASTM International, West Conshohocken, PA. https://doi.org/10.1016/0029-1021(68)90030-3

ASTM D854 (2014). *Standard Test Methods for Specific Gravity of Material Solids by Water Pycnometer*, ASTM Internatinal, West Conshohocken, PA. https://doi.org/10.1007/978-3-642-22647-2_200026

Bolton, M.D. (1986). "The strength and dilatancy of sands." *Géotechnique*, **36**(1), 65-78. https://doi.org/10.1680/geot.1986.36.1.65

Burrow, M.P.N., Bowness, D., and Ghataora, G.S. (2007). "A comparison of railway track foundation design methods." *Proceedings of Institution of Mechanical Engineers, Part F: Journal of Rail and Rapid Transit,* **221**(1), 1-12. https://doi.org/10.1243/09544097JRRT58

Burrow, M.P.N., Ghataora, G.S., and Evdorides, H. (2011). "Railway foundation design principles." *Journal of Civil Engineering and Architecture*, **5**(3), 224-232.

Dafalla, M. A. (2013). "Effects of clay and moisture content on direct shear tests for clay-sand mixtures." *Advances in Materials Science and Engineering*. Article ID. 562726 http://dx.doi.org/10.1155/2013/562726

Dareeju, B., Gallage, C., and Dhanasekar, M. (2014). "A comparative analysis of the conservative bridge transition design approaches." *Proceedings of Conference on Railway Excellence: Rail Transport for Vital Economy*, Adelaide Convention Centre, Adelaide, SA, pp. 649-657.

Dareeju, B., Gallage, C., Dhanasekar, M., and Ishikawa, T. (2016). "Cyclic plastic deformation characteristics of subgrade under moving train wheel load." *Japanese Geotechnical Society Special Publication*, **2**(46), 1619-1622. https://doi.org/10.3208/jgssp.TC202-02

Dareeju, B., Gallage, C., Ishikawa, T., and Dhanasekar, M. (2017). "Effects of principal stress axis rotation on cyclic deformation characteristics of rail track subgrade materials." *Soils and Foundations*, **57**(3), 423-438. https://doi.org/10.1016/j.sandf.2017.05.009

Gallage, C., Dareeju, B., Dhanasekar, M., and Ishikawa, T. (2016). "Effects of principal stress axis rotation on unsaturated rail track foundation deterioration." *Procedia Engineering*, **143**, 252-259. https://doi.org/10.1016/j.proeng.2016.06.032

Gräbe, P.J. and Clayton, C.R.I. (2009). "Effects of principal stress rotation on permanent deformation in rail track foundations." *Journal of Geotechnical and Geoenvironmental Engineering*, ASCE, **135**(4), 555-565. https://doi.org/10.1061/(ASCE)1090-0241(2009)135:4(555)

Gräbe, P.J. and Clayton, C.R.I. (2014). "Effects of principal stress rotation on resilient behavior in rail track foundations." *Journal of Geotechnical and Geoenvironmental Engineering*, ASCE, **140**(2), pp. 1-10. https://doi.org/10.1061/(ASCE)GT.1943-5606.0001023

Hesse, D.E., Tinjum, J.M., and Warren, B.J. (2014). "Impact of increasing freight loads on rail substructure from fracking sand transport." *Transportation Geotechnics*, **1**(4), 241-256. https://doi.org/10.1016/j.trgeo.2014.06.003

Hirakawa, D., Kawasaki, H., Tatsuoka, F., and Momoya, Y. (2002). "Effects of loading conditions on the behaviour of railway track

in the laboratory modet test." *Proceedings of the 6th International Conference on the Bearing Capacity of Roads, Railways and Airfields*, Lisbon, Portugal, pp. 1295-1305.

Holtz, R.D. and Kovacs, W.D. (1981). *An Introduction to Geotechnical Engineering*. Englewood Cliffs, N.J., Prentice-Hall.

Inam, A., Ishikawa, T., and Miura, S. (2012). "Effect of principal stress axis rotation on cyclic plastic deformation characteristics of unsaturated base course material." *Materials and Foundations*, **52**(3), 465-480. https://doi.org/10.1016/j.sandf.2012.05.006

Indraratna, B., Ionescu, D., and Christie, H. (1998). "Shear behavior of railway ballast based on large-scale triaxial tests." *Journal of Geotechnical and Geoenvironmental Engineering*, ASCE, **124**(5), 439-449. https://doi.org/10.1061/(ASCE)1090-0241(1998)124:5(439)

Indraratna, B., Khabbaz, H., and Lackenby, J. (2003). "Behaviour of railway ballast under dynamic loads based on large-scale triaxial testing." *Proceedings of AusRAIL Plus 2003*, Sydney, Australia, pp. 1-9.

Indraratna, B., Khabbaz, H., Salim, W., Lackenby, J., and Christie, D. (2004). "Ballast characteristics and the effects of geosynthetics on rail track deformation." *Proceedings of International Conference on Geosynthetics and Geoenvironmental Engineering*, Mumbai, India, pp. 5-24.

Indraratna, B., Sun, Y., and Nimbalkar, S. (2016). "Laboratory assessment of the role of particle size distribution on the deformation and degredation of ballast under cyclic loading." *Journal of Geotechnical and Geoenvironmental Engineering*, ASCE, **142**(7). 04016016 https://doi.org/10.1061/(ASCE)GT.1943-5606.0001463

Ishikawa, T. and Miura, S. (2015). "Influence of moving wheel loads on mechanical behavior of submerged coarse roadbed." *Soils and Foundations*, **55**(2), 242-257. https://doi.org/10.1016/j.sandf.2015.02.002

Ishikawa, T., Sekineo, E., and Miura, S. (2011). "Cyclic deformation of coarse material subjected to moving-wheel loads." *Canadian Geotechnical Journal*, **48**(5), 691-703. https://doi.org/10.1139/t10-099

JIS A 1224-2009, *Test Method for Minimum and Maximum Densities of Sands*, Japanese Geotechnical Society, Japan (in Japanese).

Kumara, J.J. and Hayano, K. (2016). "Deformation characteristics of fresh and fouled ballast subjected to tamping maintenance." *Soils and Foundation*, **56** (4), 652-663. https://doi.org/10.1016/j.sandf.2016.07.006

Lekarp, F., Isacsson, U., and Dawson, A. (2000). "State of the Art, I: Resilient Response of Unbound Aggregates." *Journal of Transportation Engineering*, ASCE, **126**(1), 66-75. https://doi.org/10.1061/(ASCE)0733-947X(2000)126:1(66)

Li, D. and Selig, E. (1994). "Resilient modulus for fine-grained subgrade materials." *Journal of Geotechnical Engineering*, ASCE, **120**(6), 939-957. https://doi.org/10.1061/(ASCE)0733-9410(1994)120:6(939)

Li, D. and Selig, E. (1996). "Cumulative plastic deformation for fine-grained subgrade materials." *Journal of Geotechnical Engineering*, ASCE, **122**(12), 1006-1013. https://doi.org/10.1061/(ASCE)0733-9410(1996)122:12(1006)

Li, D. and Selig, E.T. (1995). *Evaluation of Railway Subgrade Problems Railroad Transportation Research*. National Academy Press, Washington, D.C., Transportation Research Board.

Li, D. and Selig, E.T. (1998a). "Method for railroad track foundation design. I: Development." *Journal of Geotechnical and Geoenvironmental Engineering*, ASCE, **124**(4), 316-322. https://doi.org/10.1061/(ASCE)1090-0241(1998)124:4(316)

Li, D. and Selig, E.T. (1998b). "Method for railroad track foundation design. II: Applications." *Journal of Geotechnical and Geoenvironmental Engineering*, ASCE, **124**(4), 323-329. https://doi.org/10.1061/(ASCE)1090-0241(1998)124:4(323)

Li, D., Sussmann, T., Hyslip, J., and Chrismer, S. (2015). *Railway Geotechnics*, Taylor & Francis, Ltd. https://doi.org/10.1201/b18982

Likos, W. and Jaafar, R. (2013). "Pore-scale model for water retention and fluid partitioning of partially saturated coarse material." *Journal of Geotechnical and Geoenvironmental Engineering*, ASCE, **139**(5), 724-737. https://doi.org/10.1061/(ASCE)GT.1943-5606.0000811

Loh, R.B.H. and Nikarz, H.R. (2012). "Compressibility and strength of clay subgrade of railroad foundation in highly saturated condition." *Jornal of GeoEngineering*, TGS, **7**(2), 43-51. https://doi.org/10.6310/jog.2012.7(2).1

Momoya, Y., Sekine, E., and Tatsuoka, F. (2005). "Deformation characteristics of railway roadbed and subgrade under moving-wheel load." *Soils and Foundations*, **45**(4), 99-118. https://doi.org/10.3208/sandf.45.4_99

Otter, L. (2011). *The Influence of Suction Changes on the Stiffness of Railway Formation*. Ph.D. Dissertation, University of Southampton.

Powrie, W., Yang, L.A., and Clayton, C.R.I. (2007). "Stress changes in the ground below ballasted railway track during train passage." *Proceedings of Institution of Mechanical Engineers, Part F: Journal of Rail and Rapid Transit*. https://doi.org/10.1243/0954409JRRT95

Raymond, G.P. and Davies, J.R. (1978). "Triaxial tests on dolomite railroad ballast." *Journal of the Geotechnical Engineering Division*, ASCE, **104**(6), 737-751.

Shahin, M.A., Loh, R.B.H., and Nikraz, H.R. (2011). "Some observation on the behaviour of soft clay under undrained cyclic loading." *Journal of GeoEngineering*, TGS, **6**(2), 109-112. https://doi.org/10.6310/jog.2011.6(2).4

Yang, L.A., Powrie, W., and Priest, J.A. (2009). "Dynamic stress analysis of a ballasted railway track bed during train passages." *Journal of Geotechnical and Geoenvironmental Engineering*, ASCE, **135**(5), 680-689. https://doi.org/10.1061/(ASCE)GT.1943-5606.0000032